Global conservation laws and femtoscopy of small systems

Zbigniew Chajęcki* and Mike Lisa†

Department of Physics, Ohio State University, 1040 Physics Research Building, 191 West Woodruff Avenue, Columbus, Ohio 43210, USA

(Received 24 April 2008; revised manuscript received 21 July 2008; published 8 December 2008)

It is increasingly important to understand, in detail, two-pion correlations measured in $p + p$ and $d + A$ collisions. In particular, one wishes to understand the femtoscopic correlations to compare to similar measurements in heavy-ion collisions. However, in the low-multiplicity final states of these systems, global conservation laws generate significant N-body correlations that project onto the two-pion space in nontrivial ways and complicate the femtoscopic analysis. We discuss a formalism to calculate and account for these correlations in collisions dominated by a single particle species (e.g., pions). We also discuss effects on two-particle correlations between nonidentical particles, the understanding of which may be important in the study of femtoscopic space-time asymmetries.

DOI: 10.1103/PhysRevC.78.064903 PACS number(s): 25.75.Gz, 25.70.Pq, 25.40.Ve

I. INTRODUCTION

The unique and distinguishing feature of collisions between heavy ions is their large (relative to the confinement scale) size and the possibility of generating *bulk* systems, which may be described in thermodynamic terms, allowing us to discuss the equation of state of strongly interacting matter. The primary evidence for the creation of bulk matter at the highest energies [1–4] is the existence of strong collective flow [5]. The dominant feature of flow is the correlation between space and momentum it generates; thus, momentum-only observables such as p_T spectra and azimuthal anisotropies [1–4] represent only an indirect projection of the effect. Femtoscopic measurements access space as a function of particle momentum, thus providing the most direct probe of the most crucial feature of heavy-ion collisions (see, e.g., Ref. [6]). In particular, flow is manifest by a negative correlation between the "HBT radius" and the transverse mass (m_T) of the particles [7].

Clearly, then, a detailed understanding of femtoscopic measurements in heavy-ion collisions is crucial to proving the existence of, or probing the nature of, the bulk system generated in the collision. It is in fact possible to quantitatively interpret both the femtoscopic and momentum-only observations at RHIC—in $A + A$ collisions—in consistent, flow-dominated models of the system (e.g., Ref. [8]). All seems well.

However, it is important to understand the system size dependence of the apparent bulk behavior. In this paper we discuss the possible complications in the comparison of large and small systems.

A. Hadron collisions as a reference to heavy-ion collisions

One of the most exciting signals at RHIC is the modification of the jet structure caused by the bulk medium. In particular, leading particle distributions [9,10] and azimuthal correlations [11] in $A + A$ collisions are strongly suppressed relative to those from $p + p$ collisions at high p_T.

Especially since low-p_T observables directly reflect the bulk medium, it is reasonable to ask whether similar comparisons between Au + Au and $p + p$ collisions reveal comparable differences in the soft sector.

Common measurements of this type include total particle yields, p_T spectra, and azimuthal correlations (v_2). However, in each case, it is not clear whether qualitative differences between small and large systems are observed. Quantum number conservation laws in small systems can strongly affect particle yields (e.g., Refs. [12,13]). However, modulo canonical suppression effects based on equilibrium thermochemical fits to yields from $p + p$ collisions [14] produce results quite similar to those from $A + A$ collisions [15]. Blast-wave fits [8,16] to p_T spectra from $p + p$ collisions indicate sizable radial flow, though smaller than that seen in Au + Au collisions [17]. Intrinsic anisotropies from $p + p$ collisions are considered as a nonflow contribution to azimuthal correlations in $A + A$. However, it is far from obvious that the finite values of v_2 from $p + p$ collisions [18] do not arise from collective flow in the $p + p$ collision itself.

A quark-gluon plasma is usually considered a form of matter. If a quark-gluon plasma were created in $p + p$ collisions, as suggested by Bjorken [19], would it display bulk properties? A direct comparison of soft-sector observables in $p + p$ and $A + A$ collisions is necessary to address these issues [20,21]. The imminent hadronic and heavy-ion program at the LHC brings the relevance of such studies into strong relief.

B. Femtoscopy in $p + p$ collisions

More light might be brought to bear on this important question through femtoscopic measurements, which probe more directly the space-momentum correlations generated in a collective system.

Though not as plentiful as in heavy-ion collisions, two-pion femtoscopic measurements are common in $e^+ + e^-$ or $p + p(\bar{p})$ collisions [22]. In these collisions, too, "HBT radii" are

*chajecki@mps.ohio-state.edu
†lisa@mps.ohio-state.edu

observed to fall with m_T. Speculations of the physics behind this observation have included Heisenberg-uncertainty-based arguments, string-breaking phenomena, and temperature gradients; an excellent overview may be found in Ref. [23]. Preliminary measurements by the STAR Collaboration [24] even suggest that $p + p$ collisions show collective behavior similar to $A + A$ collisions. Distinguishing different physical mechanisms, however, requires a detailed understanding of the correlations themselves.

Such an understanding is complicated by the clear observation of nonfemtoscopic effects in two-pion correlations in small systems. For example, in $A + A$ collisions the functional form (Gaussian or not) fitted to two-pion correlations (e.g., Ref. [6]) incorporates only femtoscopic effects. Such fits for smaller systems (e.g., Ref. [25]) have required additional *ad hoc* terms of nonfemtoscopic nature.

C. Nonfemtoscopic correlations

Femtoscopic correlations are those that depend directly on the two-particle coordinate-space separation distribution (cf. Ref. [6]). In general, such correlations are confined to low relative velocity. Nonfemtoscopic correlations may arise from string fragmentation or global conservation laws, for example, and there is no reason to expect that such correlations appear only in kinematic regimes (e.g., ranges of relative momentum) different than the femtoscopic ones. Thus, separating those correlations may be a nontrivial exercise.

Nonfemtoscopic correlations may arise from a variety of sources. Jets will clearly induce momentum-space correlations between their fragmentation products. Although these effects may not be negligible, the low momentum of the pions under consideration ($p_T \sim 0.4$ GeV) puts us squarely in the region in which factorization breaks down and the jet interpretation becomes significantly murkier. In the kinematic region under consideration, string fragmentation may play a role; this is an area for future study, though significant model dependence will be present. Collective bulk flow (e.g., anisotropic elliptic flow) will generate N-body correlations that will project onto the two-body space. "Clusters" within events—that is, several independent particle-emitting sources—may generate additional structure [26,27]; indeed, such clusters may be treated as "large resonances" with a many-body decay channel. Each of these sources of nonfemtoscopic correlations may play a greater or lesser role in a collision, depending upon the physical scenario. In this paper, we do not focus on these sources of correlation.

In this work, we focus on effects that must be at play in any physical system: energy- and momentum-conservation-induced correlations (EMCICs). These global conservation laws provide an N-body constraint on the event, which projects down onto two-body spaces and should become more pronounced at lower event multiplicity (N).

EMCIC effects on femtoscopic correlation functions have been estimated (see Appendix C of Ref. [27]) recently in the context of a numerical model of Bose-Einstein correlations from emitting cells, using a rough but fast numerical algorithm to conserve energy-momentum. An earlier study by Bertsch *et al.* [28] included energy-momentum conservation in an analytically solvable model in the limit of one spatial dimension and nonrelativistic particles. Both studies were confined to correlation functions in one dimension of relative momentum. In this paper, effects of EMCICs on three-dimensional correlation functions are studied in detail using numerical simulations and analytic expressions, both based on the restricted phase-space integral.

D. Structure of this paper

In Sec. II we describe GENBOD, an event generator that samples an inclusive momentum distribution subject only to constraints of energy and momentum conservation. In Sec. III we briefly discuss the harmonic representation that provides a complete and natural characterization of the shape of the correlation function. An extensive discussion of symmetry constraints on the harmonics is given in Appendix B.

For the next three sections, we focus on events in which only pions are emitted. In Sec. IV we use pion-only events from GENBOD to illustrate the effects of varying constraints, frames, and kinematic cuts on EMCICs. A method to calculate analytically (but using information from measured distributions) EMCICs is shown in Sec. V. This leads to an "experimentalist's formula," given in Sec. VI, intended to disentangle EMCICs from other (e.g., femtoscopic) correlations in the data. The formula involves several approximations that may break down in reality; these are discussed and effects are evaluated quantitatively.

In Sec. VII we discuss two effects that can complicate a direct comparison of EMCICs for identical and nonidentical particle correlations. Several interesting effects are observed, which might be important for the increasingly common studies of space-time asymmetries. We find that, for nonidentical particles, the "experimentalist's formula" is only approximately applicable. We summarize our discussion in Sec. VIII.

II. CALCULATING EVENTS WITH ENERGY AND MOMENTUM CONSERVATION

To clearly understand the role of EMCICs, we would like to study events in which there is no other physics involved besides the conservation laws. Such a tool has been provided 40 years ago in the form of the GENBOD computer program (see Ref. [29] for an excellent write-up of the method and physics) in the CERN library. Given a requested total multiplicity (N), a list of masses (m_i) of emitted particles, and a total amount of energy ($E_{\rm tot}$) to distribute among them, GENBOD returns an event of random momenta (four-vectors p_j), subject only to the condition of energy and momentum conservation. More importantly, it returns, for each event, a weight proportional to the probability that the event will actually occur in nature. Thus, it is a much different tool than, say, transport codes such as RQMD [30], in which each event returned may be treated as equally probable.

This weight is based on the phase-space integral R_N [31] ,

$$R_N = \int^{4N} \delta^4\left(P - \sum_{j=1}^{N} p_j\right) \prod_{i=1}^{N} \delta\left(p_i^2 - m_i^2\right) d^4 p_i, \quad (1)$$

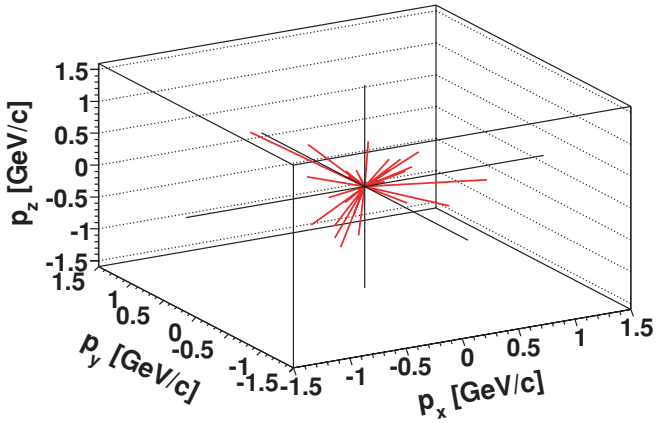

FIG. 1. (Color online) A high-probability multiplicity-30 event calculated by GENBOD. Lines correspond to particle momenta p_x, p_y, p_z.

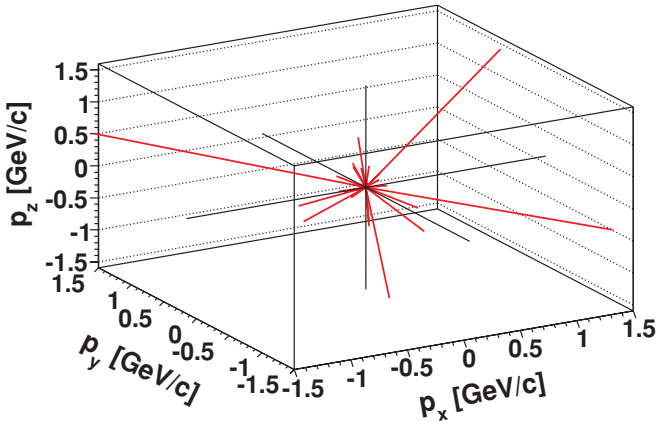

FIG. 2. (Color online) A low-probability multiplicity-30 event calculated by GENBOD. Lines correspond to particle momenta p_x, p_y, p_z.

where $P = (E_{\rm tot}, \vec{0})$ is the total momentum four-vector of the event. R_N figures dominantly in Fermi's statistical theory [32], in which the probability of having N particles in the final state is proportional to $\bar{S}_N \cdot R_N$; here $\bar{S}_N$ is the phase-space-averaged S-function (or matrix element) associated with the process generating the final state.

In the limit for which momentum distribution is dominated by phase-space restrictions alone, $\bar{S}$ is a constant, and the spectrum of a quantity α (say, an angle or transverse momentum) is given by [29,31,32]

$$f(\alpha) = \frac{d}{d\alpha} R_N. \tag{2}$$

In the limit that α represents the ensemble of momenta constituting a given event, Eq. (2) returns the event weight. See Ref. [29] for a practical iterative prescription to calculate R_N and the weights.

We select (via Monte Carlo) GENBOD events according to their weight and run them through identical software as used for experimental analysis. Fortunately, the code is fast, since one must calculate large statistics from which to select. This is because the phase-space weights vary by large factors. As a very extreme case, Figs. 1 and 2 show a likely and unlikely event, respectively, for multiplicity $N = 30$. As one would expect, the "rounder" event is more likely, though one might be surprised by the fact that the first event is a hundred million times more likely than the second one.

III. SPHERICAL HARMONIC DECOMPOSITION OF CORRELATION FUNCTIONS

Measurements of the space-time extent of a particle-emitting source at the femtometer scale is commonly done by analyzing two-particle correlation functions $C(\vec{q})$ as a function of the relative momentum $\vec{q}$. Experimentally, $C(\vec{q})$ is the ratio of the $\vec{q}$ distribution when both particles are measured in the same event to the same distribution when the two particles come from different events (see, e.g., Ref. [6] and references therein for more details). In this section, we present correlation functions produced in exactly the manner in which experimental ones are formed. GENBOD-generated events are selected according to the returned event weight.

Ideally, then, any structure remaining in this ratio reflects the correlation between particles in the same event. In the present study, these correlations come from energy and momentum conservation effects.

In this paper we will use the commonly used Bertsch-Pratt ("out-side-long") decomposition of the relative momentum $\vec{q}$ [33,34], where q_o is parallel to the transverse total momentum of the pair, q_l is parallel to the beam direction, and q_s is perpendicular to those.

Usually the three-dimensional (3-D) correlation functions are presented in one-dimensional (1-D) Cartesian projections (or slices) along these axes (e.g., q_o) with the other q-components (e.g., q_s and q_l) small. Such 1-D slices for GENBOD calculations are presented on Fig. 3. At asymptotically high relative momentum $|\vec{q}|$, femtoscopic contributions to the correlation function (those described by the Koonin-Pratt equation as discussed Ref. [6]) must approach a constant value, usually normalized to unity, independent of the direction of $\vec{q}$. Naturally, there are no femtoscopic correlations in these events; correlations induced by the global conservation laws are signaled by the nonunity value of the correlation function. The correlation function depends on the direction of $\vec{q}$ as well as $|\vec{q}|$.

However, 1-D projections represent a set of zero measure of the 3-D correlation function and are thus a poor tool for exploring its detailed and potentially important structure. In principle, one could visualize the full structure of the 3-D correlation function via a *series* of Cartesian projections in q_i over different ranges in $q_{j,k}$, where $i \neq j \neq k$. This would, however, constitute a large number of figures, and relevant patterns that cut across projections might not stand out.

By exploiting symmetries in $\vec{q}$-space, the spherical harmonic decomposition (SHD)[1] becomes a much more efficient representation that uses *all* of the data to show the shape of the

[1]Danielewicz and Pratt have studied a similar decomposition of the correlation function in terms of Cartesian harmonics [35,36].

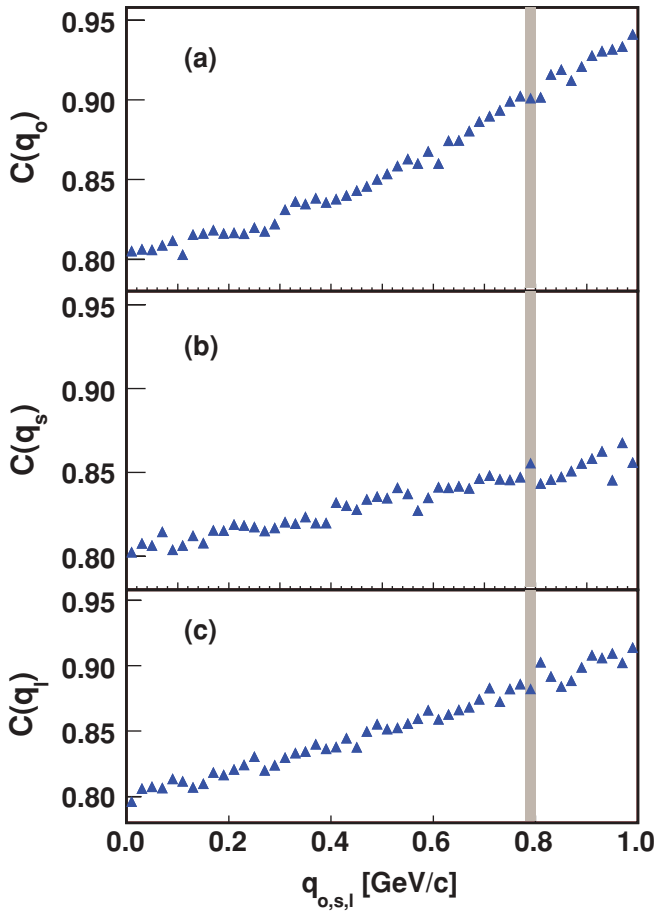

FIG. 3. (Color online) 1-D projections of 3-D correlation function calculated in LCMS frame for multiplicity-9 event calculated by GENBOD.

correlation function. Here, the spherical coordinates θ, ϕ, and $Q = |\vec{q}|$ relate to the Cartesian ones as

$$q_o = Q \sin\theta \cos\phi, \quad q_s = Q \sin\theta \sin\phi, \quad q_l = Q \cos\theta, \tag{3}$$

and we define harmonic moments $A_{l,m}$'s as

$$A_{l,m}(Q) \equiv \frac{1}{\sqrt{4\pi}} \int d\phi d(\cos\theta) C(Q,\theta,\phi) Y_{l,m}(\theta,\phi). \tag{4}$$

Usually, experimentally measured correlation functions are not continuous functions of Q, $\cos\theta$, and ϕ but are constructed with bins of finite size. In this case, Eq. (4) needs modification to account for finite-bin-size effects. For the experimental practitioner, we discuss one way to deal with this in Appendix C. For the remainder of this manuscript, we will assume these binning effects have been dealt with; that is, we assume negligible bin size in $\cos\theta$ and ϕ.

Symmetry constrains the number of relevant components. For femtoscopic analyses of identical particles at midrapidity that integrate over reaction-plane orientation (i.e., almost all analyses to date), only real parts of $A_{l,m}$'s with even values of l and m do not vanish. For the complete list of symmetries of $A_{l,m}$'s, see Appendix B. Further, it is natural to expect that the statistical relevance of high-l components is diminished.

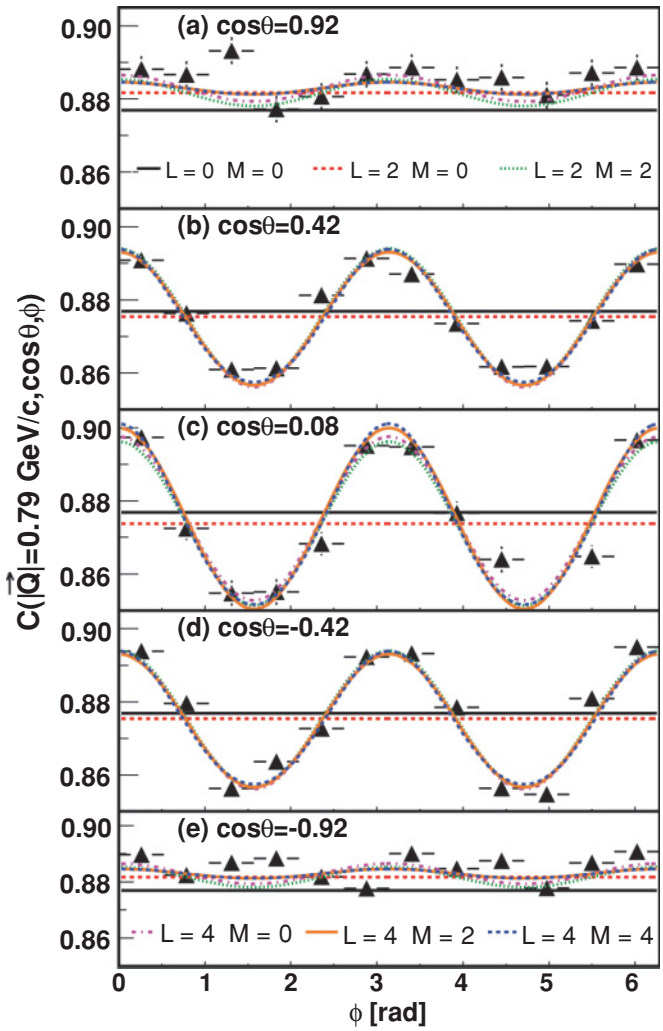

FIG. 4. (Color online) Correlation function for the same data presented in Fig. 3 shown at a fixed value of $Q = 0.79$ GeV/c (approximately indicated by the shaded region in Fig. 3) as a function of ϕ for five bins in $\cos(\theta)$. Curves represent the SHD components of various orders; see text for more details.

As an example, Fig. 4 shows the calculated correlation function (the same as shown in Fig. 3) for one value of Q as a function of $\cos\theta$ and ϕ. Also shown are curves representing SHD with increasingly higher order components. In particular, the curves correspond to

$$C_{L,M}(Q,\theta,\phi) \equiv \sqrt{4\pi} \left(\sum_{l=0}^{L-2} \sum_{m=-l}^{l} A_{l,m}(Q) Y^*_{l,m}(\theta,\phi) + \sum_{m=-M}^{M} A_{L,m}(Q) Y^*_{L,m}(\theta,\phi) \right). \tag{5}$$

For example, the curve labeled as "$L = 2$ $M = 0$" contains $A_{0,0}$ (the constant term) and $A_{2,0}$ components.

Clearly, for this example, only the first few components are required to represent the structure of the correlation function. Although a few higher l terms may be required in some cases, the number of relevant $A_{l,m}$'s is generically expected to be small. This is from general considerations of smoothness and,

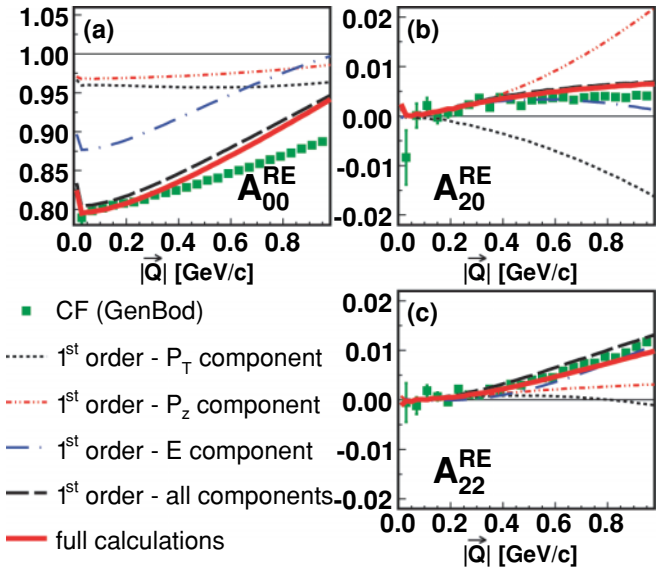

FIG. 5. (Color online) SHD coefficients for GENBOD-generated events consisting of 9 pions having average kinetic energy per particle $\bar{K} = 0.9$ GeV, as measured in the pair LCMS frame. No kinematic cuts were applied to the data. Green squares are $A_{l,m}$'s from the GENBOD events. Red solid lines are the SHD coefficients of Eq. (24) for $k = 2$. Black dotted, red dot-dash-dotted, and blue dash-dotted lines are SHD coefficients of the first, second, and third terms, respectively, of the right side of Eq. (25). Black dashed lines are SHD coefficients of the right side of Eq. (25).

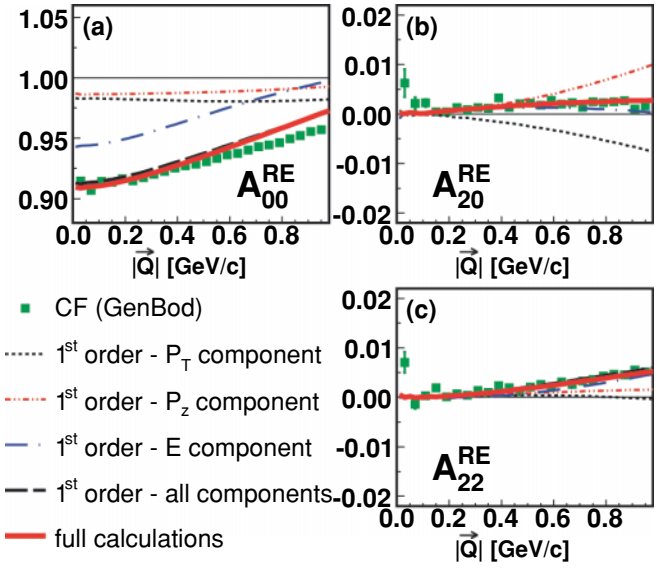

FIG. 6. (Color online) SHD coefficients for GENBOD-generated events consisting of 18 pions having average kinetic energy per particle $\bar{K} = 0.9$ GeV, as measured in the pair LCMS frame. No kinematic cuts were applied to the data. Green squares are $A_{l,m}$'s from the GENBOD events. Red solid lines are the SHD coefficients of Eq. (24) for $k = 2$. Black dotted, red dot-dash-dotted, and blue dash-dotted lines are SHD coefficients of the first, second, and third terms, respectively, of the right side of Eq. (25). Black dashed lines are SHD coefficients of the right side of Eq. (25).

for experimental data, statistical issues. Thus, by glancing at only a *few one-dimensional plots*, one views the *entire* correlation structure in orthogonal components. The number of plots is usually reduced further by symmetry constraints (cf. Appendix B).

As an example, the first few $A_{l,m}$'s for the same GENBOD calculations presented in this section are plotted as a function of Q in Fig. 5. The odd-l and odd-m moments (not shown) vanish as required by symmetry (cf. Appendix B).

IV. EMCICS FROM GENBOD

In this section, we briefly discuss factors that affect the $A_{l,m}$ moments, using Figs. 5–10. For the present, we focus only on the green squares, labeled "CF (GenBod)," in those figures.

Figures 5, 6, and 7 show the $A_{l,m}$'s calculated in the longitudinally co-moving system (LCMS) frame [6] from GENBOD events that have the same average kinetic energy per particle ($\bar{K} = 0.9$ GeV) but different multiplicity. As expected, the strength of the EMCICs decreases with event multiplicity. Similarly, for a given event multiplicity, one expects larger EMCICs when there is less available energy. As shown in Figs. 6 and 8 for multiplicity-18 events, this is indeed the case.

Since the definition of the "out," "side," and "long" directions—and thus the angles θ and ϕ—depend on the frame of measurement, one expects the spherical harmonic coefficients $A_{l,m}$ to depend on reference frame. This is shown in Figs. 6 and 9 for correlations measured in LCMS and pair center of mass (CMS) frames.

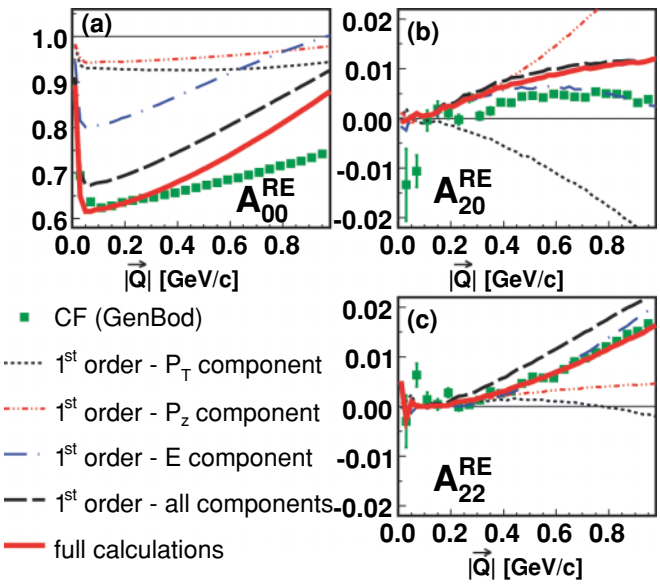

FIG. 7. (Color online) SHD coefficients for GENBOD-generated events consisting of 6 pions having average kinetic energy per particle $\bar{K} = 0.9$ GeV, as measured in the pair LCMS frame. No kinematic cuts were applied to the data. Green squares are $A_{l,m}$'s from the GENBOD events. Red solid lines are the SHD coefficients of Eq. (24) for $k = 2$. Black dotted, red dot-dash-dotted, and blue dash-dotted lines are SHD coefficients of the first, second, and third terms, respectively, of the right side of Eq. (25). Black dashed lines are SHD coefficients of the right side of Eq. (25).

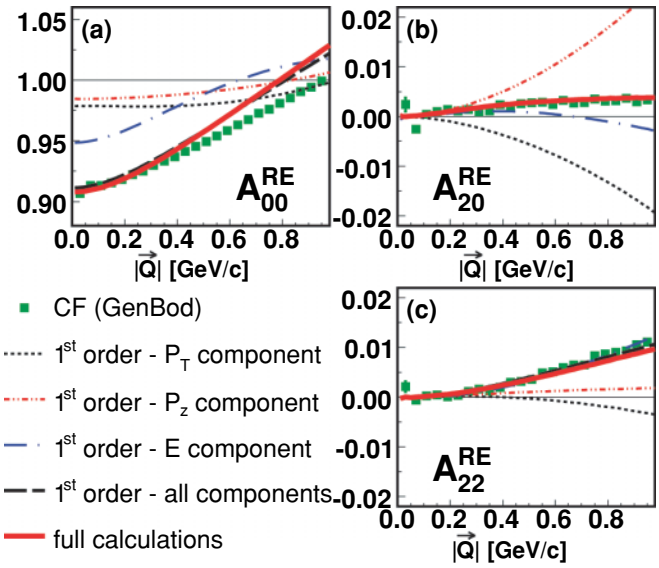

FIG. 8. (Color online) SHD coefficients for GENBOD-generated events consisting of 18 pions having average kinetic energy per particle $\bar{K} = 0.5$ GeV, as measured in the pair LCMS frame. No kinematic cuts were applied to the data. Green squares are $A_{l,m}$'s from the GENBOD events. Red solid lines are the SHD coefficients of Eq. (24) for $k = 2$. Black dotted, red dot-dash-dotted, and blue dash-dotted lines are SHD coefficients of the first, second, and third terms, respectively, of the right side of Eq. (25). Black dashed lines are SHD coefficients of the right side of Eq. (25).

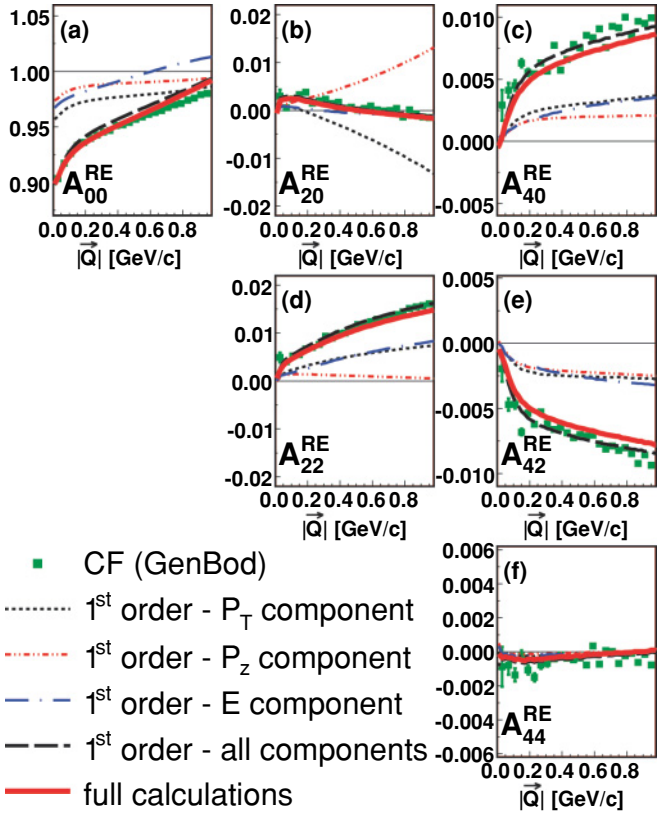

FIG. 9. (Color online) SHD coefficients for GENBOD-generated events consisting of 18 pions having average kinetic energy per particle $\bar{K} = 0.9$ GeV, as measured in the pair CMS frame. No kinematic cuts were applied to the data. Green squares are $A_{l,m}$'s from the GENBOD events. Red solid lines are the SHD coefficients of Eq. (24) for $k = 2$. Black dotted, red dot-dash-dotted, and blue dash-dotted lines are SHD coefficients of the first, second, and third terms, respectively, of the right side of Eq. (25). Black dashed lines are SHD coefficients of the right side of Eq. (25).

Less intuitive is the observation that the correlation strength depends also on kinematic cuts. Figures 9 and 10 show the $A_{l,m}$'s calculated by GENBOD for 18-pion events without and with a selection of $|\eta| < 0.5$, respectively. (Note that this cut applies to the pions that are used in the analysis, *not* to the set of particles for which energy and momentum is conserved; energy and momentum is always conserved for the full event.)

Finally, we note two important and generic effects. First, EMCICs are present at all values of $|\vec{Q}|$, reminding us that we cannot (responsibly) ignore these effects in a femtoscopic analysis. Second, in Figs. 9 and 10, we have included $A_{l,m}$ components up to $l = 4$. Typically, $|A_{l+2,m}/A_{l,m}| \sim 0.1$, another reminder that characterization of the three-dimensional correlation function requires only a few harmonic components.

V. ANALYTIC CALCULATION OF EMCICS

Even if EMCIC effects generated by GENBOD "resemble" the experimental data, it is likely unwise to use GENBOD itself to correct the data for several reasons. First, there is strong sensitivity to the (not completely measured) number and species mix of *all* particles emitted in the event, including neutrinos and possible magnetic monopoles (or, less exotically, particles escaping detector acceptance). Second, there is strong sensitivity to the energy "available" in the event; it is not obvious that this is $\sqrt{s_{NN}}$ of the collision. Third, EMCIC effects depend on the individual momenta $\vec{p}_1$ and $\vec{p}_2$ of the particles entering the correlation function. This will depend on acceptance, efficiency, kinematic cuts, and, to a degree, the underlying single-particle phase space. (Whereas correlation functions are insensitive to the single-particle phase space, the correlations they measure may, in fact, depend on this phase space, owing to physical effects.)

Thus, one would like to calculate EMCICs based on the data themselves. In this section, we begin by following arguments similar to those in Refs. [37–39] to obtain correction factors that implement EMCICs onto multiparticle distributions. In the course of the calculation, we make some simplifying approximations. The derived expressions are then tested for accuracy against the numerical GENBOD simulations. Finally, the expressions are used to extract an "experimentalist's formula" discussed in the next section.

A. Restricted phase-space corrections

Danielewicz [37], and later Borghini, Dinh, and Ollitrault [38], considered EMCIC-type effects on two-particle azimuthal correlations (quantified by v_2 and often used as a measure of elliptic flow [5]). They focused mostly on transverse momentum ($\vec{P}_T$) conservation only, but Borghini

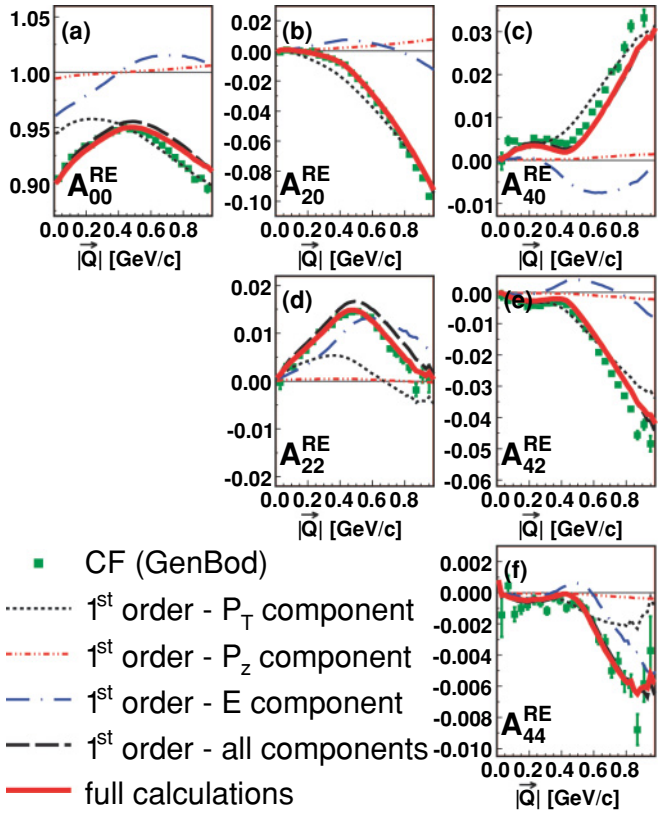

FIG. 10. (Color online) SHD coefficients for GENBOD-generated events consisting of 18 pions having average kinetic energy per particle $\bar{K} = 0.9$ GeV, as measured in the pair CMS frame. Only particles with $|\eta| < 0.5$ are used in the correlation function. Green squares are $A_{l,m}$'s from the GENBOD events. Red solid lines are the SHD coefficients of Eq. (24) for $k = 2$. Black dotted, red dot-dash-dotted, and blue dash-dotted lines are SHD coefficients of the first, second, and third terms, respectively, of the right side of Eq. (25). Black dashed lines are SHD coefficients of the right side of Eq. (25).

later [39] generalized to the case of an arbitrary number of independent (orthogonal) spatial dimensions and recently considered momentum conservation effects on three-particle analyses of jetlike behavior [40].

As we shall see in the following, for correlation functions used in femtoscopy, conservation of energy generates effects of similar magnitude to those from conservation of (three-) momentum. We deal only with on-shell particles, for which energy *cannot* be treated as independent of the momentum (as, say, p_x would be largely independent of p_y). Thus, unlike the aforementioned works, we will explicitly begin with the more general multivariate central limit theorem.

We start with the case of interest—$D = 3$ spatial dimensions—and conserve three-momentum $\vec{p}$. We implement energy conservation and on-shell constraints a bit later.

We define[2]

$$f(\vec{p}_i) \equiv \frac{d^3N}{d\vec{p}_i^3} \tag{6}$$

as the single-particle momentum distribution unaffected by EMCICs. This may be considered the unmeasured "parent" distribution. Then, the k-particle distribution (k less than the total multiplicity N) including EMCICs is

$$f_c(\vec{p}_1, \ldots, \vec{p}_k) = \left(\prod_{i=1}^{k} f(\vec{p}_i)\right) \frac{\int \left(\prod_{j=k+1}^{N} d^3\vec{p}_j f(\vec{p}_j)\right) \delta^3\left(\sum_{i=1}^{N} \vec{p}_i\right)}{\int \left(\prod_{j=1}^{N} d^3\vec{p}_j f(\vec{p}_j)\right) \delta^3\left(\sum_{i=1}^{N} \vec{p}_i\right)}. \tag{7}$$

Note the difference between numerator and denominator in the starting value of the index j on the product.

We implement total energy conservation $\sum E_i = \sqrt{s}$, by replacing $\delta^3(\sum_{i=1}^{N} \vec{p}_i) \to \delta^4(\sum_{i=1}^{N} p_i - P)$ in Eq. (7). Here, $P = (\sqrt{s}, \vec{0})$ is the total energy-momentum of the event, and $p_{0,i} = E_i = \sqrt{\vec{p}_i^2 + m_i^2}$ is the energy of the on-shell particle.

We denote Lorentz-invariant distributions as

$$\tilde{f}(p_i) \equiv 2E_i \frac{d^3N}{d\vec{p}_i^3} = 2E_i f(p_i) \tag{8}$$

and rewrite Eq. (7) as

[2]Our use of symbols f and f_c follows the convention used in Ref. [38], which is significantly different than (if unfortunately similar looking to) that used in Refs. [39] and [40].

$$\begin{aligned}
\tilde{f}_c(p_1, \ldots, p_k) &= \left(\prod_{i=1}^{k} \tilde{f}(p_i)\right) \frac{\int \left(\prod_{j=k+1}^{N} \frac{d^3\vec{p}_j}{E_j} \tilde{f}(\vec{p}_j)\right) \delta^4\left(\sum_{i=1}^{N} p_i - P\right)}{\int \left(\prod_{j=1}^{N} \frac{d^3\vec{p}_j}{E_j} \tilde{f}(\vec{p}_j)\right) \delta^4\left(\sum_{i=1}^{N} p_i - P\right)} \\
&= \left(\prod_{i=1}^{k} \tilde{f}(p_i)\right) \frac{\int \left(\prod_{j=k+1}^{N} d^4p_j \delta\left(p_j^2 - m_j^2\right) \tilde{f}(p_j)\right) \delta^4\left(\sum_{i=1}^{N} p_i - P\right)}{\int \left(\prod_{j=1}^{N} d^4p_j \delta\left(p_j^2 - m_j^2\right) \tilde{f}(p_j)\right) \delta^4\left(\sum_{i=1}^{N} p_i - P\right)} \\
&= \left(\prod_{i=1}^{k} \tilde{f}(p_i)\right) \frac{\int \left(\prod_{j=k+1}^{N} d^4p_j g(p_j)\right) \delta^4\left(\sum_{i=1}^{N} p_i - P\right)}{\int \left(\prod_{j=1}^{N} d^4p_j g(p_j)\right) \delta^4\left(\sum_{i=1}^{N} p_i - P\right)}.
\end{aligned} \tag{9}$$

Thus, we arrive at an integral over four independent variables, in which the integrand function $g(p)$ is "highly peaked" and with strong correlations in the 4-D p-space.

According to Eq. (9), the k-body momentum distribution, including EMCICs, is the k-body distribution *not* affected by EMCICs (i.e., just an uncorrelated product of single-particle distributions) multiplied by a "correction factor," which enforces the EMCIC. The numerator of this factor counts the number of configurations in which the remaining $N-k$ on-shell particles conspire to conserve total energy and momentum, and the denominator normalizes the distribution.

B. Application of the central limit theorem

To arrive at a useful result, we argue along lines similar to those of Refs. [37–39]. The distribution of a large number M of uncorrelated momenta $W=\sum_{i=1}^{M} p_i$ is, by the central limit theorem (CLT), a multivariate normal distribution

$$\begin{aligned} &F_M(W) \\ &\quad\equiv \int \left(\prod_{i=1}^{M} d^4p_i\, g(p_i)\right) \delta^4\left(\sum_{i=1}^{M} p_i - W\right) \\ &\quad= \sqrt{\frac{|B|}{(2\pi)^4}}\exp\left(-\frac{1}{2}\left(W^\mu - \langle P^\mu\rangle\right) B_{\mu\nu}\left(W^\nu - \langle P^\nu\rangle\right)\right). \end{aligned} \tag{10}$$

Here, the average of the sum of four-momenta is simply related to the single-particle average of the four-momenta as

$$\langle P^\mu\rangle = \sum_{i=1}^{M}\left\langle p_i^\mu\right\rangle = M\left\langle p_i^\mu\right\rangle, \tag{11}$$

where

$$\begin{aligned} \langle p_\mu^n\rangle &\equiv \frac{\int d^4p\, g(p)\cdot p_\mu^n}{\int d^4p\, g(p)}, \\ \langle p_\mu p_\nu\rangle &\equiv \frac{\int d^4p\, g(p) p_\mu p_\nu}{\int d^4p\, g(p)}. \end{aligned} \tag{12}$$

Finally, in Eq. (10), $|B|$ denotes the determinant of the matrix B. Up to a factor of M, B is the inverse of the covariance matrix of the distribution $g(p)$:

$$B_{\mu\nu} = \frac{1}{M} b_{\mu\nu}, \tag{13}$$

$$(b^{-1})_{\mu\nu} = \langle p_\mu p_\nu\rangle - \langle p_\mu\rangle\langle p_\nu\rangle. \tag{14}$$

We can now apply the CLT by recognizing the integral in the numerator in Eq. (9) as the distribution of $N-k$ momenta $\sum_{j=k+1}^{N} p_j = P - \sum_{j=1}^{k} p_j$ so that for "large enough" $N-k$, we find

$$\begin{aligned} &\tilde{f}_c(p_1,\ldots,p_k) \\ &\quad= \left(\prod_{i=1}^{k}\tilde{f}(p_i)\right)\frac{F_{N-k}\left(P-\sum_{i=1}^{k} p_i\right)}{F_N(P)} \\ &\quad= \left(\prod_{i=1}^{k}\tilde{f}(p_i)\right)\cdot\left(\frac{N}{N-k}\right)^2 \exp\left[-\left(\sum_{i=1}^{k}\left(p_i^\mu - \langle p^\mu\rangle\right)\right)\right. \\ &\qquad\left.\times\frac{b_{\mu\nu}}{2(N-k)}\left(\sum_{i=1}^{k}\left(p_i^\nu - \langle p^\nu\rangle\right)\right)\right]. \end{aligned} \tag{15}$$

It is appropriate at this point to repeat the two approximations we have employed up to now. The first assumption, always important in using the CLT, is that $N-k$ is sufficiently large; recall that N is the total multiplicity and k is the order of the correlation being calculated ($k=2$ for two-particle correlations). Second, we have implicitly assumed that all particles in the system are governed by the *same* single-particle distribution $g(p)$. Strictly speaking, then, the system must consist of particles all of the same mass, and if there are several species with the same mass (say, π^- and π^+), they must furthermore have the same momentum distribution. This is at best an approximation for hadron or ion collisions, in which other particles contribute to the pion-dominated final state.

C. Observable EMCIC effects

Even the single-particle momentum distribution is affected by EMCICs:

$$\begin{aligned} &\tilde{f}_c(p_i) \\ &\quad= \tilde{f}(p_i)\cdot\left(\frac{N}{N-1}\right)^2 \\ &\qquad\times\exp\left[-\left(p^\mu - \langle p^\mu\rangle\right)\frac{b_{\mu\nu}}{2(N-k)}\left(p^\nu - \langle p^\nu\rangle\right)\right]. \end{aligned} \tag{16}$$

The product of such a single-particle distribution forms the denominator of the k-particle correlation function

$$\begin{aligned} &C(p_1,\ldots,p_k) \\ &\quad\equiv \frac{\tilde{f}_c(p_1,\ldots,p_k)}{\tilde{f}_c(p_1)\cdots\tilde{f}_c(p_k)} = \frac{\left(\frac{N}{N-k}\right)^2}{\left(\frac{N}{N-1}\right)^{2k}} \\ &\qquad\times\frac{\exp\left[\frac{-1}{2(N-k)}\sum_{i,j=1}^{k}\left(p_i^\mu - \langle p^\mu\rangle\right)b_{\mu\nu}\left(p_j^\nu - \langle p^\nu\rangle\right)\right]}{\exp\left[\frac{-1}{2(N-1)}\sum_{i=1}^{k}\left(p_i^\mu - \langle p^\mu\rangle\right)b_{\mu\nu}\left(p_i^\nu - \langle p^\nu\rangle\right)\right]}. \end{aligned} \tag{17}$$

In this paper we concentrate on correlation functions in $q_{\rm out}$, $q_{\rm side}$ and $q_{\rm long}$, as is done in femtoscopic studies. However, the two-particle correlation function in relative azimuthal angle, which probes elliptic flow, may also contain EMCIC contributions through Eq. (17). These effects turn out to be small and are discussed in Appendix A.

To first order in $1/N$, the two-particle correlation function becomes

$$C(p_1,p_2) = 1 - \frac{1}{N}\left(p_1^\mu - \langle p^\mu\rangle\right)b_{\mu\nu}\left(p_2^\nu - \langle p^\nu\rangle\right). \tag{18}$$

The multivariate CLT used in Sec. V B accounts for correlations between vector components via the covariance matrix b^{-1} [Eq. (14)], which has, in general, 10 nonvanishing

elements. The average vector P [Eq. (11)] has in general four nonvanishing elements. We now reduce these numbers significantly by considering the specific case of our interest.

First, we choose to work in the global center-of-momentum frame, so that

$$\langle p^\mu \rangle = \delta_{\mu,0} \langle E \rangle. \tag{19}$$

For the correlations, we are interested in signals generated by EMCICs alone, not, for example, dynamical correlations resulting from flow. Neglecting elliptic flow (azimuthal anisotropies in the parent distribution [5,41]) implies

$$(b^{-1})_{1,2} = \langle p_x p_y \rangle = 0. \tag{20}$$

The same approach was adopted in earlier work [37,38,40]. Similarly, we assume no dynamical correlations from directed flow [41], implying

$$(b^{-1})_{1,3} = \left(b^{-1}\right)_{2,3} = 0. \tag{21}$$

The on-shell constraint generates an unavoidable dependence between energy and three-momentum components. However, in the CLT limit, only the second moment (covariance) comes into play, and this vanishes. For $i \neq 0$,

$$\begin{aligned}(b^{-1})_{0,i} &= \langle E p_i \rangle - \langle E \rangle \langle p_i \rangle = \langle E p_i \rangle \\ &= \frac{\int dE \int d^3\vec{p} \cdot E g(p) \cdot p_i}{\int dE \int d^3\vec{p} \cdot g(p)} = 0.\end{aligned} \tag{22}$$

In the last step, we recognize that p_i is an odd function of momentum, whereas E and g are even.

In this scenario of interest, then, b is diagonal, and Eq. (16) becomes

$$\tilde{f}_c(p_i) = \tilde{f}(p_i) \cdot \left(\frac{N}{N-1}\right)^2 \exp\left[-\frac{1}{2(N-1)} \times \left(\frac{p_{i,x}^2}{\langle p_x^2 \rangle} + \frac{p_{i,y}^2}{\langle p_y^2 \rangle} + \frac{p_{i,z}^2}{\langle p_z^2 \rangle} + \frac{(E_i - \langle E \rangle)^2}{\langle E^2 \rangle - \langle E \rangle^2}\right)\right]. \tag{23}$$

Similarly, Eq. (17) becomes

$$\begin{aligned}&C(p_1, \ldots, p_k) \\ &\equiv \frac{\tilde{f}_c(p_1, \ldots, p_k)}{\tilde{f}_c(p_1) \cdots \tilde{f}_c(p_k)} = \frac{\left(\frac{N}{N-k}\right)^2}{\left(\frac{N}{N-1}\right)^{2k}} \\ &\times \frac{\exp\left[\frac{-1}{2(N-k)} \left\{\sum_{\mu=1}^3 \left(\frac{\left(\sum_{i=1}^k p_{i,\mu}^2\right)^2}{\langle p_\mu^2 \rangle}\right) + \frac{\left(\sum_1^k (E_i - \langle E \rangle)\right)^2}{\langle E^2 \rangle - \langle E \rangle^2}\right\}\right]}{\exp\left[\frac{-1}{2(N-1)} \sum_{i=1}^k \left\{\sum_{\mu=1}^3 \frac{p_{i,\mu}^2}{\langle p_\mu^2 \rangle} + \frac{(E_i - \langle E \rangle)^2}{\langle E^2 \rangle - \langle E \rangle^2}\right\}\right]}\end{aligned} \tag{24}$$

and Eq. (18) becomes

$$C(p_1, p_2) = 1 - \frac{1}{N}\left(2\frac{\vec{p}_{1,T} \cdot \vec{p}_{2,T}}{\langle p_T^2 \rangle} + \frac{p_{1,z} \cdot p_{2,z}}{\langle p_z^2 \rangle} + \frac{(E_1 - \langle E \rangle)(E_2 - \langle E \rangle)}{\langle E^2 \rangle - \langle E \rangle^2}\right), \tag{25}$$

where we have taken $\langle p_x^2 \rangle = \langle p_y^2 \rangle = \langle p_T^2 \rangle / 2$ in the azimuthally symmetric case of interest. In what follows and in Figs. 5–10, we shall refer to the first, second, and third terms within the parentheses of Eq. (25) as the "p_T," "p_z," and "E" components, respectively.

If we somehow know N, $\langle p_T^2 \rangle$, $\langle p_z^2 \rangle$, $\langle E^2 \rangle$, and $\langle E \rangle$, we can calculate EMCICs using Eq. (24). (See, however, the discussion at the start of the next section.) Better yet, if N is large enough, then we can use Eq. (25). This is what is done in Figs. 5–10. The open circles and orange inverted triangles represent the results of Eq. (24) and Eq. (25), respectively. The black circles, blue stars, and red triangles show the individual components of Eq. (25); this decomposition will be relevant when we discuss the "experimentalist's formula" in the next section.

Figures 5–10 make clear that each of the three terms in Eq. (25) produces nontrivial behavior of the $A_{l,m}$'s. Also clear is the importance of not neglecting the energy term. We find also that the p_z term affects $A_{2,2}$; this may be surprising since $A_{2,2}$ quantifies the behavior of the correlation function in the "out-side" plane, whereas $\hat{z}$ is the "long" direction in the Bertsch-Pratt system. Clearly, EMCICs projected onto a two-particle space are nontrivial objects.

The first-order expansion [Eq. (25)] agrees well with the full expression [Eq. (24)] for $N \gtrsim 10$. Such multiplicities are relevant for $p + p$ measurements at RHIC (where we recall that N includes all particles, even unmeasured ones). We see also that the analytic calculations (open circles and inverted triangles) approximate the results of the GENBOD simulation (green squares), especially as the multiplicity and total energy of the event increases; increasing agreement for large N and E_{tot} is expected, given the approximations leading to our analytic expressions. We observe also that the analytically calculated expressions respond identically to the kinematic cuts as does the simulation (cf. Figs. 9 and 10).

Finally, the analytic calculations never reproduce *exactly* the simulations; we discuss this further in the next section.

VI. AN EXPERIMENTALIST'S FORMULA

Even for large N and energy, the calculations do not exactly reproduce the EMCIC effects in the simulation. One reason for this may be found, in fact, in the definition of the average values (e.g., $\langle p_z^2 \rangle$) themselves. In Eq. (12), average quantities are calculated by using the distribution $\tilde{f}(p)$, which is not affected by EMCICs. Naturally, the only measurable distribution available to the experimentalist (even when GENBOD simulations serve as the "experiment") is $\tilde{f}_c(p)$.

Thus, it appears that experimentalists cannot plug their data into Eqs. (12) and (25) to fully calculate EMCICs. However, such an ambition would have been hopeless anyhow. After all, even the total multiplicity N (again, including photons, etc.) is rarely fully measured, and in principle N is a number of "primary" particles, a murky concept in itself.

To the practicing femtoscopist, there is a natural solution. Having at hand (1) educated guesses for the quantities N, $\langle E^2 \rangle$, etc. and (2) a physically motivated functional form that connects these quantities to the correlations, one may perform

a fit. Let us rewrite Eq. (25) as

$$C(p_1, p_2) = 1 - M_1 \cdot \overline{\{\vec{p}_{1,T} \cdot \vec{p}_{2,T}\}} - M_2 \cdot \overline{\{p_{1,z} \cdot p_{2,z}\}} - M_3 \cdot \overline{\{E_1 \cdot E_2\}} + M_4 \cdot \overline{\{E_1 + E_2\}} - \frac{M_4^2}{M_3}, \tag{26}$$

where

$$M_1 \equiv \frac{2}{N\langle p_T^2\rangle}, \quad M_2 \equiv \frac{1}{N\langle p_z^2\rangle}, \quad M_3 \equiv \frac{1}{N(\langle E^2\rangle - \langle E\rangle^2)}, \quad M_4 \equiv \frac{\langle E\rangle}{N(\langle E^2\rangle - \langle E\rangle^2)}. \tag{27}$$

The notation $\overline{\{X\}}$ in Eq. (26) highlights the fact that X is a two-particle quantity that depends on p_1 and p_2 (or $\vec{q}$, etc.). From a practical point of view, X will be averaged over the same $\vec{q}$ bins as used for the correlation function. For infinitesimally narrow q bins, $\overline{\{X\}} = X$. The binned functions $\overline{\{X\}}$ then automatically reflect the same event and particle selection as the correlation function. This involves nothing more than adding four more histograms to the several already being constructed by the experimentalist in processing pairs in the data.

Here, we should emphasize that, in Eq. (26), $\vec{p}_1$, E_1, $\vec{p}_2$, and E_2 should be calculated in the collision center-of-momentum (CCM) frame. The reason is that Eq. (9) [hence Eqs. (10)–(27)] assumes some fixed total energy and momentum to be conserved. The event's total energy and momentum [hence $\langle E\rangle$, $\langle \vec{p}\rangle$, etc. appearing in Eqs. (10)–(27)] are fixed quantities in any given frame. In a *pair*-dependent frame (e.g., LCMS), the total energy and momentum of the event will fluctuate, pair-by-pair. Thus, although the correlation function may be *binned* in whatever frame one chooses, the momenta p_i^μ on the right side of Eqs. (9)–(27) must be calculated in a pair-independent frame. In fact, starting with Eq. (19), we have chosen the CCM, for simplicity.

The parameters M_i defined in Eq. (27), however, are global and independent of p_1 and p_2. It is these which we will use as fit parameters. The task is then fast and straightforward; the EMCIC part of the correlation function $C(\vec{q})$ is simply a weighted sum of four functions. Indeed, one may calculate coefficients as in Eq. (4) for the four new functions. For example,

$$A_{l,m}^{p_z}(Q) \equiv \sum_{\text{bins } i} \overline{\{p_{1,z} \cdot p_{2,z}\}}(Q, \cos\theta_i, \phi_i) \cdot Y_{l,m}(\cos\theta_i, \phi_i), \tag{28}$$

etc. Then, because of the linearity of Eq. (26) and the orthonormality of the $Y_{l,m}$'s, the measured $A_{l,m}$'s themselves are similarly just weighted sums of harmonics,

$$A_{l,m}(Q) = \delta_{l,0} \cdot \left(1 - M_4^2/M_3\right) - M_1 \cdot A_{l,m}^{p_T}(Q) - M_2 \cdot A_{l,m}^{p_z}(Q) - M_3 \cdot A_{l,m}^{(E\cdot E)}(Q) + M_4 \cdot A_{l,m}^{(E+E)}(Q). \tag{29}$$

Treating Eq. (29) as a fit, we have a few (say six, for $l \leqslant 4$) *one*-dimensional functions to fit with four adjustable weights. The number of degrees of freedom in this four-parameter fit remains high: ~ 300, for six $A_{l,m}$'s, each with 50 bins in $|Q|$.

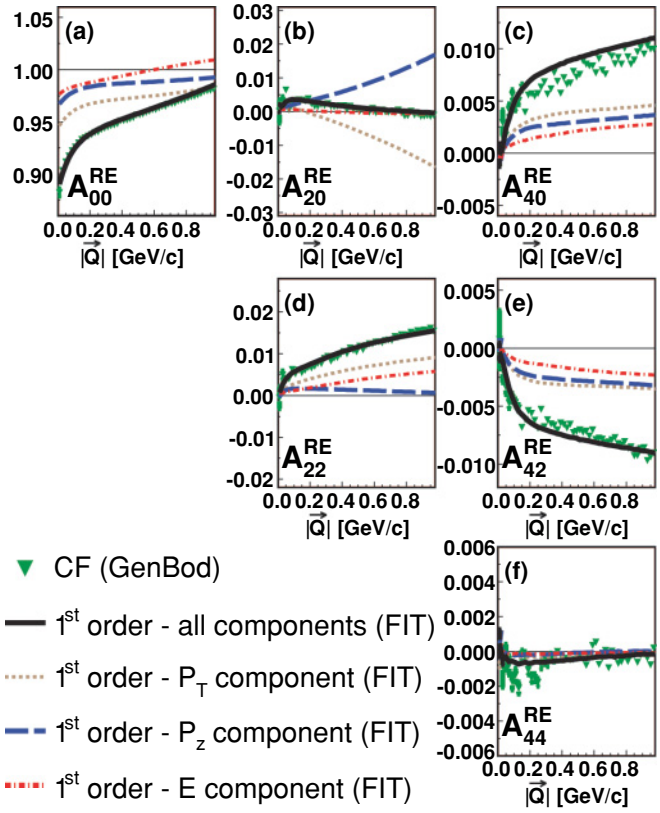

FIG. 11. (Color online) Green inverted triangles show the π-π^- correlation function, in the pair rest frame, from 18-pion GENBOD-generated events. The black curve is a result of a fit with the "experimentalist's formula" from Eq. (29). Other curves represent the three component terms of the fit: $M_1 \cdot A_{l,m}^{p_T}(Q)$ in the brown dotted line; $M_2 \cdot A_{l,m}^{p_z}(Q)$ in the blue dashed line; and $M_3 \cdot A_{l,m}^{E\cdot E}(Q) + M_4 \cdot A_{l,m}^{E+E}(Q)$ in the red dash-dot line. See text for details.

An example is shown in Fig. 11, where GENBOD-calculated correlation functions are fitted with the form of Eq. (29). Not surprisingly, the minimization procedure returned fit parameters M_i very close to the values calculated via Eq. (27). However, exact agreement between the "best" parameter values returned by the fit and those from Eq. (27) is not expected. This is because the large-N approximation is only approximately valid and because $\tilde{f}(p) \neq \tilde{f}_c(p)$, as discussed previously. Treating the M_i as adjustable parameters leads to a slightly different weighting of the terms and a slightly better fit to the data.

Our original goal was not to understand EMCICs *per se*, but to extract the femtoscopic information from measured two-particle correlations. Assuming that the only nonfemtoscopic correlations are EMCICs, one may simply add the femtoscopic terms $\Phi_{\text{femto}}(p_1, p_2)$ to the fitting function in Eq. (26) or (29):

$$C(p_1, p_2) = \Phi_{\text{femto}}(p_1, p_2) \times \left(1 - M_1 \cdot \overline{\{\vec{p}_{1,T} \cdot \vec{p}_{2,T}\}} - M_2 \cdot \overline{\{p_{1,z} \cdot p_{2,z}\}}\right.$$

$$- M_3 \cdot \overline{\{E_1 \cdot E_2\}} + M_4 \cdot \overline{\{E_1 + E_2\}} - \frac{M_4^2}{M_3}\Big). \tag{30}$$

Common femtoscopic fitting functions (e.g., Gaussian in the out-side-long space) usually contain ∼five parameters (e.g., $N, \lambda, R_i, i = o, s, l$). In the imaging technique [42], one assumes the separation distribution is described by a sum of splines, rather than a Gaussian; here, too, there are usually four or five fit parameters (spline weights). So, by including EMCIC effects, we have roughly doubled the number of fit parameters, relative to a "traditional" fit, which ignores them. This is a nontrivial increase in analysis complexity. However, we keep in mind two points.

First, the increased effort is simply necessary. EMCICs (and possibly other important nonfemtoscopic correlations) are present and increasingly relevant at low multiplicity. One option is to ignore them, as has sometimes been done in early high-energy experiments. However, with the new high-quality data and desire for detailed understanding at RHIC, ignoring obvious features such as those presented in Ref. [43] is clearly unacceptable. Perhaps a slightly better option is to invent an *ad hoc* functional form [25] without a strong real physical basis. We hope that the results here present a relatively painless and more reasonable third option.

Second, whereas the nonfemtoscopic EMCICs are not confined to the large-Q region (an important point!), the femtoscopic correlations are confined to the small-Q region. Therefore, one hopes that the addition of four new parameters to the fit of the correlation function will not render the fit overly unwieldy. Although we cannot expect complete block-diagonalization of the fit covariance matrix, one hopes that the M_i are determined well enough at high Q that the femtoscopic fit parameters can be extracted at low Q.

VII. NONIDENTICAL PARTICLE CORRELATIONS

For at least two reasons, it is important to turn attention to correlations between nonidentical particles.

First, it is natural to ask whether one can use other particle combinations to "correct" for effects of EMCICs in, say, identical-pion correlation functions. After all, EMCICs are induced by global constraints on the entire event, not a specific particle species. For example, various experiments have explored using (π^+, π^-) correlations to account for EMCICs in (π^+, π^+) correlation functions [44–46].

Second, it is also important to know whether EMCICs could cloud the interpretation of correlations between nonidentical particles. It is increasingly common to study asymmetries in the correlation functions of, say π-K pairs [47], interpreting such as a "shift" in the average point of emission between the two particles [48]. In the spherical harmonic decomposition, such shifts appear in the $l = 1$ moments (cf. Appendix B). We will find that EMCICs can indeed generate an asymmetry that might naively be considered proof of a femtoscopic shift.

Here we discuss two effects—one immediately obvious and one more subtle—that are relevant to these issues. The discussion is broken into three parts. Neglecting EMCICs and any other source of correlation at first, we briefly show the effects of two common resonances on correlations between oppositely charged pions in a toy model. Thus calibrated, we use the more realistic and complex PYTHIA model to illustrate a nontrivial interplay between EMCICs and the resonances, which can mock up a femtoscopic asymmetry signal. Finally, we return to a toy model—now with nonidentical particles and EMCICs, but without resonances or the several other sources of correlation present in PYTHIA—to make clear the mechanism behind the special effects EMCICs have on nonidentical particle correlations.

A. Effect of resonances

First we consider the effect of resonances. To focus on effects other than global EMCICs we use a toy model in which only 10 identical resonances per event are generated but no other particles are produced. The momentum of each resonance is generated from a thermal distribution; energy and momentum are conserved for each decay separately, but not globally for the whole event.

Figure 12 shows the spherical harmonic moments of (π^+, π^-) correlation functions for events including ω (blue squares) and ρ resonances (red triangles).

As seen, even without considering EMCICs, the correlations among particles coming from resonance decays produce

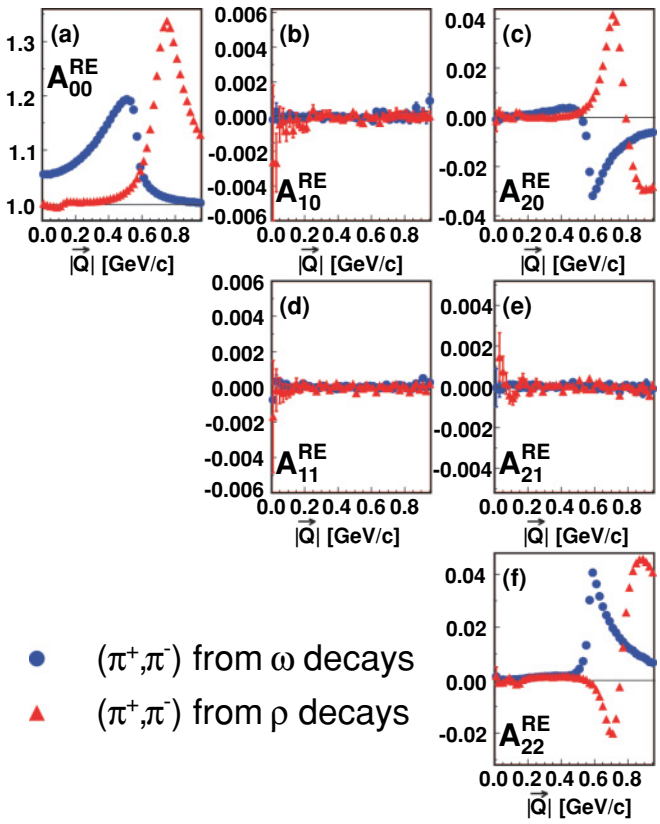

FIG. 12. (Color online) (π^+, π^-) correlation functions calculated in the LCMS frame for events including ω (blue squares) and ρ (red triangles) resonances.

nontrivial structure. In this case, one cannot simply divide the (π^+,π^+) correlation function by (π^+,π^-) to "remove" EMCICs.

B. Entrance channel asymmetries

In addition to the correlation between daughters of resonance decays (cf. Fig. 12), there is a more subtle effect to consider. This happens when the two particles have different inclusive momentum distributions *and* energy and momentum are globally conserved. Under these conditions nonidentical particle correlations exhibit structure absent in identical particle correlations.

Figure 13 shows PYTHIA [49] calculations of (π^+,π^-) correlations for $p+p$ and $p+\bar{p}$ collisions at 200 GeV. In addition to obvious correlations between daughters of resonance decays (K^0_s, ω, ρ), we see additional structure. We focus on the structure in the $l=1$ moments. In general, such moments need not vanish for correlations of nonidentical particles, as discussed in Appendix B.

Correlations between sibling daughters of ρ and ω resonance decay do not generate $l=1$ moments, as seen in Sec. VII A. However, pions that are daughters of these decays will in general have a different single-particle momentum distribution than pions from other sources in the event. If the fraction of pions from resonance decay, as a function of pion momentum, is different for π^+ and π^-, then the single-particle distributions of positive and negative pions will be different. We argue in the following that it is this difference in single-particle distributions that is the key to the nonvanishing $l=1$ moments; that this difference may arise from resonances in the case at hand is irrelevant.

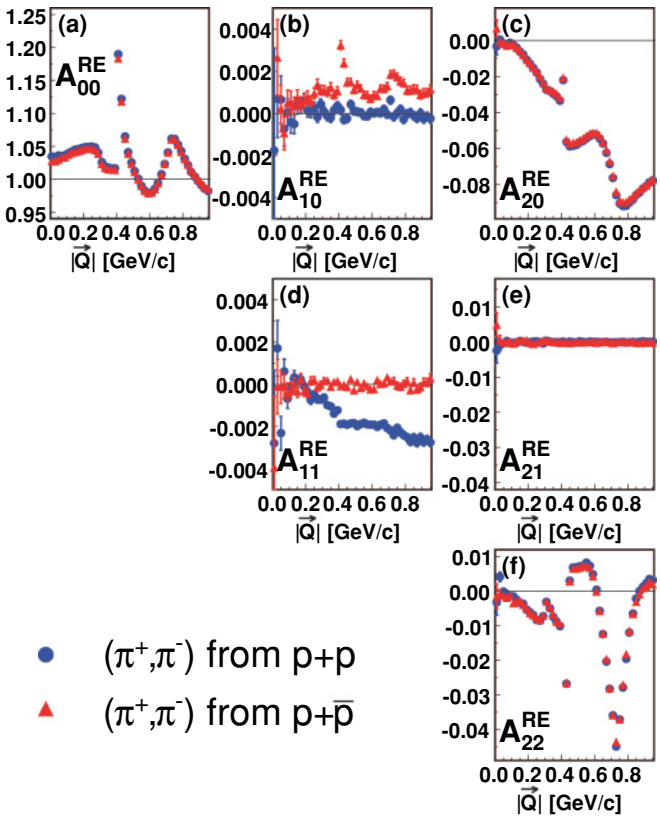

FIG. 13. (Color online) SHD moments of (π^+,π^-) correlation function from $p+p$ and $p+\bar{p}$ collisions at 200 GeV calculated from PYTHIA events.

In the $p+\bar{p}$ collisions, the fraction of π^+ coming from any given source (e.g., ρ decay) must be identical to that of π^-, for a given value of p_T. Thus the p_T distribution of π^- must be identical to that of π^+. However, the rapidity distributions will be mirror images of each other. Thus, any asymmetry in π-π^+ correlations from $p+\bar{p}$ collisions will be associated with $q_{\rm long}$ and will appear in $A_{1,0}$, as seen in Fig. 13. Similarly, the vanishing (nonvanishing) moment $A_{1,0}(A_{1,1})$ for $p+p$ collisions reflects the fact the single-particle distributions will show no asymmetry in rapidity but may differ as a function of p_T.

Since single-particle distributions divide out of a correlation function, a difference between π^+ and π^- momentum distributions, by itself, cannot generate a signal in $A_{l,m}$'s. Rather, a global correlation, coupled with this difference, generates the signal. We discuss this further in the following.

C. A simpler case

In Sec. VII B, we argued that the small difference in single-particle momentum distributions between positive and negative pions produced by PYTHIA, coupled with global conservation laws, generated nontrivial EMCICs in the nonidentical particle correlations. However, PYTHIA contains many non-EMCIC sources of correlations, related to string fragmentation and other processes, that might be flavor or isospin dependent. To make clearer our argument, we here show a simple GENBOD simulation, containing both pions and protons, but no explicit correlations between them such as a Δ resonance. Owing at least to their different masses, $\tilde{f}_{\rm proton} \neq \tilde{f}_{\rm pion}$ is guaranteed.

Figures 14 shows the π-p correlation function. Since the underlying single-particle proton and pion distributions are isotropic, $A_{1,0}$ [sensitive to shape elongation in $C(\vec{q})$ in q_l relative to transverse components] is expected to vanish. $A_{1,1}$ is finite, however, owing to differences in p_T distributions. Since there is no other source of correlation in the simulation, this obviously is an EMCIC.

From Fig. 14 it is also clear that neither Eq. (24) nor its first-order expansion [Eq. (25)] fully describes the correlation function. This is because our formalism is built on the assumption that all particles in the system follow the same parent distribution, as pointed out after Eq. (12).

VIII. SUMMARY

To truly claim an understanding of the bulk nature of matter at RHIC and the LHC, a detailed picture of the dynamically generated geometric substructure of the system created in heavy-ion collisions is needed. It is believed that this substructure, and the matter itself, is dominated by strong collective flow. The most direct measure of this flow is a measurement of the space-momentum correlation [e.g., $R(m_T)$] it

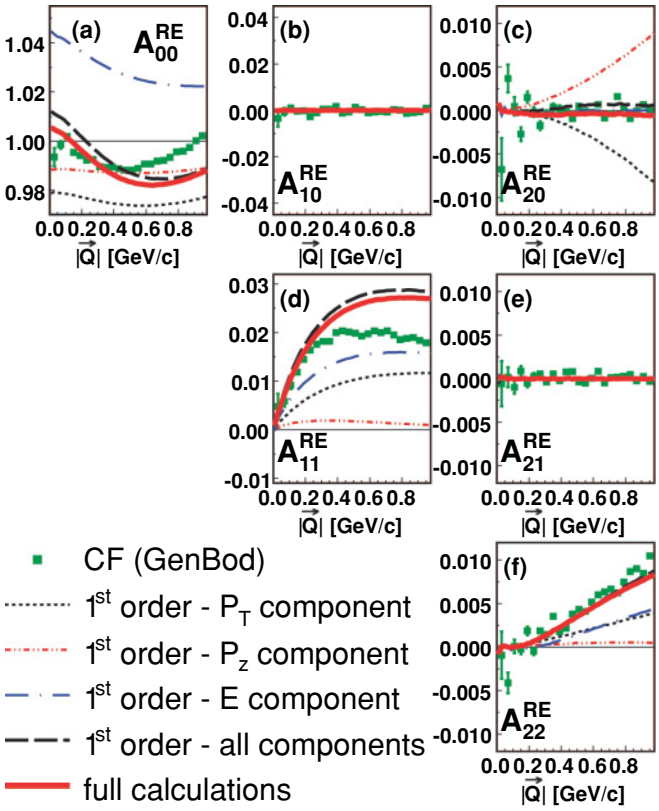

FIG. 14. (Color online) Green squares show the π-p correlation function, in the pair rest frame, from GENBOD-generated events. Red solid lines are the SHD coefficients of Eq. (24) for $k = 2$. Black dotted, red dot-dash-dotted, and blue dash-dotted lines are SHD coefficients of the first, second, and third terms, respectively, of the right side of Eq. (25). Black dashed lines are SHD coefficients of the right side of Eq. (25).

generates. The physics of this large system, and the signals it generates, should be compared to the physics dominating $p + p$ collisions, as is increasingly important in high-p_T studies at RHIC. For small systems, however, nonfemtoscopic effects contribute significantly to the correlation function, clouding the extraction and interpretation of femtoscopic ones.

We have discussed a spherical harmonic representation of the correlation function that clearly separates components of the three-dimensional shape measured in modern experiments. This representation is maximally efficient, inasmuch as only a few 1-Dl plots need be examined to extract full 3-D shape information. The relevant number of such plots is further reduced from symmetry conditions, discussed in detail in Appendix B.

EMCICs, correlations generated by kinematic conservation laws, are surely present and increasingly relevant as the event multiplicity is reduced. Using the code GENBOD to study correlation functions solely driven by EMCICs, we found highly nontrivial 3-D structures strongly influenced by event characteristics (multiplicity and energy) and kinematic particle selection.

We extended the work of Danielewicz, Ollitrault, and Borghini to include four-momentum conservation and applied it to correlation functions commonly used in femtoscopy. We found structures associated individually with the conservation of the four-momentum components, which interfere in nontrivial ways. Comparison of the analytic EMCIC calculations with the GENBOD simulation gave confidence that the approximations (e.g., "large" multiplicity N) entering into the calculation were sufficiently valid, at least for the multiplicities considered here. We further showed that the full EMCIC calculation can safely be replaced with a first-order expansion in $1/N$.

Based on this first-order expansion, we developed a practical, straightforward "experimentalist's formula" to generate histograms from the data that are later used in a generalized fit to the measured correlation function, including EMCICs and femtoscopic correlations. The degree to which this functional form fully describes measured experimental correlation functions has not been discussed and will need exploration on a case-by-case basis.

There is strong interest in correlations between nonidentical particles, for two reasons. First, sometimes π-π^- correlations are divided by π^+-π^- correlations in an attempt to "divide out" EMCICs. (In such a procedure, resonance regions are avoided, naturally.) We discussed potential problems with such an approach, related to entrance-channel asymmetries coupled with EMCICs. Secondly, 3-D asymmetries (sometimes quantified as "double ratios"; e.g., see Ref. [47]) in the correlation function for different-mass particles (e.g., π-K) are often interpreted in terms of dynamically generated differences in the average space-time emission point between the two particles. Using a very simple example, we discussed that EMCICs might significantly cloud such an interpretation.

The huge systematics of results and interest in femtoscopy in heavy-ion collisions is renewing similar interest in the space-time signals from $p + p$ collisions. Direct comparisons between the two systems are now possible at RHIC and have already produced intriguing preliminary results. Very soon, $p + p$ collisions will be measured in the LHC experiments, and the heavy-ion experimentalists will be eager to apply their tools. The femtoscopic tool is one of the best in the box—so long as we keep it sufficiently calibrated with respect to nonfemtoscopic effects increasingly relevant in small systems.

ACKNOWLEDGMENTS

We wish to thank Drs. Mark Baker, Nicolas Borghini, Paweł Danielewicz, Ulrich Heinz, Adam Kisiel, Konstantin Mikhaylov, Dariusz Miśkowiec, Jean-Yves Ollitrault, Alexey Stavinsky, and Boris Tomášik for important suggestions and insightful discussions. We would also like to thank an anonymous referee for useful suggestions to Sec. V. This work is supported by the U.S. National Science Foundation under Grant No. PHY-0653432.

APPENDIX A: EMCIC EFFECTS ON v_2

Since EMCICs can produce a structure in the correlation function even in the absence of femtoscopic correlations, it

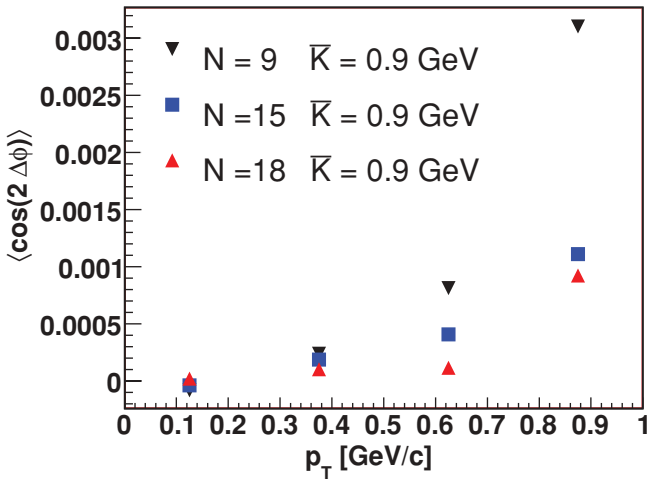

FIG. 15. (Color online) $v_2(p_T)$ for different event multiplicities. See text for details.

is worthwhile to check analytically and then confirm with simulations whether v_2—a common measure of collective elliptic flow [5]—may be affected by EMCICs.

When calculating flow from two-particle correlations we have the following relations:

$$\int \cos(m\Delta\phi)\cos(n\Delta\phi)d\Delta\phi = \delta_{m,n}\pi, \tag{A1}$$

where for v_2, $n = 2$.

This means that in the absence of flow all EMCIC terms vanish except for the ones that exhibit $\cos(2\Delta\phi)$ dependence of $\Delta\phi$. For example, in the first-order expansion of EMCICs [see Eq. (24)] there is a term $\vec{p}_{T,1}\vec{p}_{T,1} \sim \cos(\Delta\phi)$. This term gives no contribution to v_2, nor do any other terms from $1/N$ expansion. The first term that gives a nonzero contribution to v_2 [which means goes like $\cos(2\Delta\phi)$] is the second-order expansion term in $\vec{p}_T$, which is proportional to $(\vec{p}_{T,1}\vec{p}_{T,1})^2 \sim \cos^2(\Delta\phi) \sim \cos(2\Delta\phi)$. This term (as well as a few other terms in higher order $1/N$ expansions) will give a nonzero contribution to v_2. In our GENBOD simulations we do not have a flow so we can study the magnitude of the EMCIC effects on v_2 measurements. Such results are presented in Fig. 15, where we plot v_2 versus p_T for three different event multiplicities while the free kinetic energy per particle is fixed ($\bar{K} = 0.9$ GeV).

As seen, the magnitude of a nonflow contribution to v_2 from EMCICs is getting smaller with increasing multiplicity and even for low-multiplicity events the magnitude is of order of a few per mile for large p_T. From this dependence we can predict that this effect will be so small in heavy-ion collisions that it can be simply neglected.

APPENDIX B: SYMMETRY CONSIDERATIONS

The spherical harmonic decomposition representation, in which three-dimensional correlation functions are represented by several one-dimensional moments, $A_{l,m}$, efficiently condenses the shape information. A much greater increase in efficiency comes, however, with the realization that many $A_{l,m}$'s must vanish by symmetry, depending on the cuts and conditions of the analysis. Besides reducing information by significant factors, this realization also provides diagnostic power—nonphysical artifacts often appear in $A_{l,m}$'s that do not vanish when they should. Digging out such effects in the traditional 3-D Cartesian representation can be quite difficult.

In the most general case, the 3-D correlation function may have any shape, with no symmetry constraints. In this case, none of the $A_{l,m}$'s need vanish. Usually, however, an analysis is less than fully general, and symmetry consequences then arise.

In particular, we will consider four common conditions used in practice:

(i) One measures correlations between identical particles.
(ii) The measurement covers a symmetric rapidity region about $y = 0$ and the collision is between identical ions (e.g., Au + Au rather than Au + Si).
(iii) The measurement is integrated over reaction-plane angle.
(iv) The measurement might be correlated with the *second*-order reaction plane, but the first-order reaction plane is not known. In other words, the direction of the impact parameter is known at best only modulo π.

Our strategy begins by identifying transformations in relative momentum $\vec{q}$ under which the measured correlation must be invariant. As an example, since the overall sign of $\vec{q}$ is meaningless when discussing pairs of identical particles (condition (i)), $C(q_o, q_o, q_l) = C(-q_o, -q_o, -q_l)$, or, in spherical coordinates, $C(Q, \cos\theta, \phi) = C(Q, -\cos\theta, \phi - \pi)$.

We then use a symmetry of the spherical harmonics, here $Y_{l,m}(\cos\theta, \phi) = (-1)^l Y_{l,m}(-\cos\theta, \phi + \pi)$ to find

$$\begin{aligned}
A_{l,m}(Q) &\equiv \frac{1}{4\pi}\int_0^{2\pi} d\phi \int_{-1}^{1} d\cos\theta C(Q, \cos\theta, \phi) \\
&\quad \times Y_{l,m}(\cos\theta, \phi) \\
&= \frac{1}{4\pi}\int_0^{2\pi} d\phi \int_{-1}^{1} d\cos\theta C(Q, -\cos\theta, \phi - \pi) \\
&\quad \times Y_{l,m}(\cos\theta, \phi) \\
&= \frac{1}{4\pi}\int_{-\pi}^{\pi} d\phi \int_{1}^{-1} (-d\cos\theta) C(Q, \cos\theta, \phi) \\
&\quad \times Y_{l,m}(-\cos\theta, \phi+\pi) \\
&= \frac{1}{4\pi}\int_0^{2\pi} d\phi \int_{-1}^{1} d\cos\theta C(Q, \cos\theta, \phi)(-1)^l \\
&\quad \times Y_{l,m}(\cos\theta, \phi) \\
&= (-1)^l A_{l,m}(Q).
\end{aligned} \tag{B1}$$

Thus, all odd-l moments $A_{l,m}$ must vanish for correlations between identical particles.

The same type of reasoning is used in the following in identifying symmetry constraints for various combinations of analysis conditions.

TABLE I. The possible transformations (numbered in the left column) in which the signs of $\vec{q}$ components flip and the effect of the transformation on the $Y_{l,m}$'s.

#	Transformation	$Y_{l,m}$ consequence
0	$(q_o, q_s, q_l) \to (+q_o, +q_s, +q_l)$	$Y_{l,m} \to Y_{l,m}$
1	$(q_o, q_s, q_l) \to (+q_o, +q_s, -q_l)$	$Y_{l,m} \to (-1)^{l+m} Y_{l,m}$
2	$(q_o, q_s, q_l) \to (+q_o, -q_s, +q_l)$	$Y_{l,m} \to Y^*_{l,m}$
3	$(q_o, q_s, q_l) \to (+q_o, -q_s, -q_l)$	$Y_{l,m} \to (-1)^{l+m} Y^*_{l,m}$
4	$(q_o, q_s, q_l) \to (-q_o, +q_s, +q_l)$	$Y_{l,m} \to (-1)^{m} Y^*_{l,m}$
5	$(q_o, q_s, q_l) \to (-q_o, +q_s, -q_l)$	$Y_{l,m} \to (-1)^{l} Y^*_{l,m}$
6	$(q_o, q_s, q_l) \to (-q_o, -q_s, +q_l)$	$Y_{l,m} \to (-1)^{m} Y_{l,m}$
7	$(q_o, q_s, q_l) \to (-q_o, -q_s, -q_l)$	$Y_{l,m} \to (-1)^{l} Y_{l,m}$

A. $\vec{q}$ transformations and $Y_{l,m}$ response

Table I lists all combinations in which one or more of the components of $\vec{q}$ can change sign. For later reference, the transformations are numbered $0, \ldots, 7$, according to a binary scheme. The effect of the transformation on the spherical harmonics appears in the last column of the table.

Transformation (0), of course, is the trivial identity transformation, under which any correlation function is invariant, and which imposes no symmetry constraint. We include it in the table only for completeness and do not discuss it further.

B. Restrictions, invariants, and consequences on $A_{l,m}$'s

Under which of the transformations in Table I does the correlation function remain invariant? Since identical-particle correlations are more common than correlations between nonidentical particles, there will be a greater familiarity with the symmetries of the former. Thus, we begin with this more familiar case and then discuss nonidentical particle correlations. Our observations are collected in Table II.

1. Correlations between identical particles

To systematically identify those transformations in Table I that leave a correlation function invariant, it helps to have a concrete functional form to discuss. For identical pions, the correlation function is often parametrized as a Gaussian with six "radius" parameters,

$$C(q_o, q_o, q_l) = 1 + \lambda \cdot \exp\big(- R_o^2 q_o^2 - R_s^2 q_s^2 - R_l^2 q_l^2 - 2R_{os}^2 q_o q_s - 2R_{ol}^2 q_o q_l - 2R_{sl}^2 q_s q_l \big). \quad \text{(B2)}$$

Whereas measured correlation functions often have non-Gaussian features not captured by this parametrization, the form given in Eq. (B2) contains the generic and most general symmetries of all correlation functions using identical particles. Thus, we use this familiar example to focus the discussion. The six parameters in Eq. (B2) describe an ellipsoid described by three axis lengths and rotated by three

TABLE II. Symmetry consequences of analysis conditions. The left four columns show various combinations of analysis cuts and conditions, identified (i)–(iv) as discussed in the beginning of this Appendix. [Note that condition (iii) implies condition (iv); this is indicated by the symbol (√) in column (iv).] The middle seven columns indicate the consequent invariance symmetries of the correlation function according to the numbering scheme of Table I. The right-most column indicates which, if any, spherical harmonic moments of the correlation function must vanish.

Conditions				$C(\vec{q})$ invariances							Which $A_{l,m}$'s vanish
(i)	(ii)	(iii)	(iv)	1	2	3	4	5	6	7	
√										√	l odd
√	√									√	l odd
√		√	(√)		√			√		√	Re$[A_{l,m}]$: l odd Im$[A_{l,m}]$: $\forall\, l, m$
√	√	√	(√)	√	√	√	√	√	√	√	Re$[A_{l,m}]$: l and/or m odd Im$[A_{l,m}]$: $\forall l, m$
√			√							√	l odd
√	√		√	√					√	√	l and/or m odd
											–
	√										–
		√	(√)		√						Im$[A_{l,m}]$: $\forall l, m$
	√	√	(√)	√	√	√					Re$[A_{l,m}]$: odd $(l+m)$ Im$[A_{l,m}]$: $\forall l, m$
			√								–
	√		√	√							odd $(l+m)$

Euler angles in $\vec{q}$-space. Measured examples are shown and discussed in Ref. [50].

Clearly, the form of Eq. (B2) is invariant under transformation (7), as discussed earlier. Invariance under any of transformations (1)–(6) requires that one or more of the "radius" parameters R^2_{ij} vanish. In general, none of them do [50,51], even when a region symmetric about midrapidity in a collision between identical ions (condition (ii)) is considered.[3]

If the measurement is integrated over reaction-plane angle, then the "side" direction has no relevant sign, $R^2_{os} = R^2_{sl} = 0$, and the correlation function is invariant under transformation (2). Although R^2_{ol} need not vanish [53], the correlation function is unchanged if q_o and q_l change sign together [transformation (5)].

Further constraining the measurement to a symmetric region about midrapidity implies also that R^2_{ol} vanish, and the correlation function is then invariant under all transformations (0)–(7). This is the most common set of measurement conditions.

At high energies, it is common only to determine the second-order reaction plane. This corresponds to condition (iv). If the measurement is performed at midrapidity (condition (ii)), then R^2_{os} is the only nonvanishing cross-term radius, so the correlation function is invariant under transformation (1). Away from midrapidity, R^2_{ol} need not vanish, so (7) is again the only remaining transformation leaving $C(\vec{q})$ invariant.

2. *Correlations between nonidentical particles*

Correlations between nonidentical particles are no longer invariant under transformation (7), as they may depend on odd-power terms of the components of $\vec{q}$. In the case of femtoscopic correlations, the strengths of these odd powers probe asymmetries in the average emission point between the two particle species [48].

From a symmetry standpoint, the correlation function will be characterized by nine parameters, rather than the six "HBT radii" of Eq. (B2). In the simple case that $C(q_o, q_o, q_l)$ would be Gaussian, these new parameters might represent the offset from the origin of the ellipsoid in $\vec{q}$-space.

In the absence of any cuts—or if only the midrapidity condition (ii) is applied [3]—all nine parameters may take any value, and there are no required invariances or symmetry constraints. If the reaction plane is integrated over (condition (iii)) then $C(q_o, q_o, q_l)$ may remain sensitive to the sign of q_o (reflecting, for example, a different average time of emission between the particles [48]) and q_l (reflecting the difference in emission point in the beam direction, for analyses away from midrapidity), but not q_s, since an angle-averaged physical source must be symmetric with respect to the beam axis.

Unlike the case in which it is the sole condition, if the midrapidity condition (ii) is imposed *together* with condition (iii), then it does have an effect. In particular, a dependence on the sign of q_l vanishes.

If condition (iii) is relaxed to condition (iv) (i.e., the analysis is sensitive to the second-order reaction plane), then the sign of q_s may matter. This is because the sign of q_o always affects correlations between nonidentical particles and, as in identical particle correlations in which R^2_{os} may be finite, so the sign of $q_o q_s$ may separately matter. Thus, imposition of condition (iv) alone implies no symmetry constraints.

[3] At first, it seems surprising that, in the absence of reaction-plane assumptions, no additional symmetry constraint is imposed onto the correlation function by a symmetric selection about midrapidity (i.e., none of the "radius" parameters R^2_{ij} are required to vanish). However, the selection does impose symmetry constraints at a "higher" level. In identical-particle correlations, for example, although R^2_{ol} need not vanish at midrapidity for any given measured correlation function, symmetry demands a relationship between R^2_{ol} measured in different correlation functions; in particular $R^2_{ol}(\phi_{K,\mathrm{RP}} + \pi) = -R^2_{ol}(\phi_{K,\mathrm{RP}})$, where $\phi_{K,\mathrm{RP}}$ is the angle between the total pair momentum and the reaction plane. Symmetries at this level are discussed in detail in Ref. [52].

APPENDIX C: FINITE BINNING EFFECTS

Equation (4) defines the harmonic moments in terms of a continuous correlation function. Most experimentally measured correlation functions are constructed via histograms with discrete, finite bins. For decomposition into spherical harmonics, a natural choice would be to use bins in Q, $\cos\theta$ and ϕ [cf. Eq. (3)]. Here, we will find an approximate expression, analogous to Eq. (4), for the harmonic moments in terms of the discretized correlation function.

We denote the fixed bin sizes in the angular coordinates as $\Delta_{\cos\theta}$ and Δ_ϕ. Binning in Q is unimportant here, since Q is carried as an explicit argument in both C and $A_{l,m}$. The binned correlation function (denoted with superscript Δ) is related to the continuous one as

$$\begin{aligned}
&C^{\Delta}(Q, \cos\theta_i, \phi_i) \\
&\quad = \frac{1}{\Delta_\phi \Delta_{\cos\theta}} \int_{\phi_i - \Delta_\phi/2}^{\phi_i + \Delta_\phi/2} d\phi \int_{\cos\theta_i - \Delta\cos\theta/2}^{\cos\theta_i + \Delta\cos\theta/2} d(\cos\theta) \\
&\qquad \times C\,(Q, \cos\theta, \phi) \\
&\quad = \frac{\sqrt{4\pi}}{\Delta_\phi \Delta_{\cos\theta}} \sum_{l'=0}^{\infty} \sum_{m'=-l'}^{+l'} A_{l',m'}(Q) \\
&\qquad \times \int_{\phi_i - \Delta_\phi/2}^{\phi_i + \Delta_\phi/2} d\phi \int_{\cos\theta_i - \Delta_{\cos\theta}/2}^{\cos\theta_i + \Delta_{\cos\theta}/2} d(\cos\theta) Y^*_{l',m'}(\cos\theta, \phi) \\
&\quad = \sqrt{4\pi} \sum_{l'=0}^{\infty} \sum_{m'=-l'}^{+l'} A_{l',m'}(Q) \cdot F_{l',m'}(\Delta_\phi, \Delta_{\cos\theta}, \cos\theta_i) \\
&\qquad \times Y^*_{l',m'}(\cos\theta_i, \phi_i). \qquad \text{(C1)}
\end{aligned}$$

Here,

$$\begin{aligned}
&F_{l',m'}(\Delta_\phi, \Delta_{\cos\theta}, \cos\theta_i) \\
&\quad = \frac{\sin(m\Delta_\phi/2)}{m\Delta_\phi/2} \frac{1}{\Delta_{\cos\theta} P_{l',m'}(\cos\theta_i)} \\
&\qquad \times \int_{\cos\theta_i - \Delta_{\cos\theta}/2}^{\cos\theta_i + \Delta_{\cos\theta}/2} d(\cos\theta) P_{l',m'}(\cos\theta) \qquad \text{(C2)}
\end{aligned}$$

is the term that includes the finite binning effects.

Assuming that $A_{l,m}$'s vanish for l, m greater than the sampling Nyquist frequency, by the sampling theorem [54,55], the $A_{l,m}$'s are completely determined by C^{Δ}. In fact, if $F_{l,m}$ were independent of $\cos\theta_i$, then we would have

$$A_{l,m}(Q) = \frac{\Delta_\phi \Delta_{\cos\theta}}{F_{l,m}\left(\Delta_{\cos\theta}, \Delta_\phi\right)\sqrt{4\pi}} \times \sum_{\text{bins } i} C^{\Delta}\left(Q, \cos\theta_i, \phi_i\right) Y_{l,m}\left(\cos\theta_i, \phi_i\right),$$

where the summation is over all bins of $\cos\theta$ and ϕ for a given Q.

However, $F_{l,m}$ does depend on $\cos\theta_i$, so this equation does not strictly hold. Nevertheless, we find, numerically, that an excellent approximation is

$$A_{l,m}(Q) \approx \frac{\Delta_\phi \Delta_{\cos\theta}}{\sqrt{4\pi}} \sum_{\text{bins } i} \frac{C^{\Delta}\left(Q, \cos\theta_i, \phi_i\right) Y_{l,m}\left(\cos\theta_i, \phi_i\right)}{F_{l,m}\left(\Delta_{\cos\theta}, \Delta_\phi, \cos\theta_i\right)}. \tag{C3}$$

For any given measurement, one may check the validity of this approximation by plugging the result of Eq. (C3) into the expression on the last line of Eq. (C1). To the extent that it returns the measured correlation function C^{Δ}, the $A_{l,m}$'s returned by Eq. (C3) are correctly extracted. If there are deviations, the correct $A_{l,m}$'s can be found by iterative techniques.

Other methods to remove binning effects have also been proposed [56].

[1] J. Adams *et al.* (STAR Collaboration), Nucl. Phys. **A757**, 102 (2005).
[2] K. Adcox *et al.* (PHENIX Collaboration), Nucl. Phys. **A757**, 184 (2005).
[3] B. B. Back *et al.*, Nucl. Phys. **A757**, 28 (2005).
[4] I. Arsene *et al.* (BRAHMS Collaboration), Nucl. Phys. **A757**, 1 (2005).
[5] J.-Y. Ollitrault, Phys. Rev. D **46**, 229 (1992).
[6] M. Lisa, S. Pratt, R. Soltz, and U. Wiedemann, Annu. Rev. Nucl. Part. Sci. **55**, 311 (2005).
[7] S. Pratt, Phys. Rev. Lett. **53**, 1219 (1984).
[8] F. Retiere and M. A. Lisa, Phys. Rev. C **70**, 044907 (2004).
[9] S. S. Adler *et al.* (PHENIX Collaboration), Phys. Rev. Lett. **91**, 072301 (2003).
[10] J. Adams *et al.* (STAR Collaboration), Phys. Rev. Lett. **91**, 172302 (2003).
[11] C. Adler *et al.* (STAR Collaboration), Phys. Rev. Lett. **90**, 082302 (2003).
[12] C. Derreth, W. Greiner, H. T. Elze, and J. Rafelski, Phys. Rev. C **31**, 1360 (1985).
[13] H. T. Elze and W. Greiner, Phys. Lett. **B179**, 385 (1986).
[14] F. Becattini and U. Heinz, Z. Phys. C **76**, 269 (1997).
[15] P. Braun-Munzinger, D. Magestro, K. Redlich, and J. Stachel, Phys. Lett. **B518**, 41 (2001).
[16] E. Schnedermann, J. Sollfrank, and U. W. Heinz, Phys. Rev. C **48**, 2462 (1993).
[17] J. Adams *et al.* (STAR Collaboration), Phys. Rev. Lett. **92**, 112301 (2004).
[18] J. Adams *et al.* (STAR Collaboration), Phys. Rev. C **72**, 014904 (2005).
[19] J. D. Bjorken, FERMILAB-PUB-82-059-THY.
[20] R. M. Weiner, Int. J. Mod. Phys. E **15**, 37 (2006).
[21] S. M. Troshin and N. E. Tyurin, hep-ph/0609248.
[22] G. Alexander, Rep. Prog. Phys. **66**, 481 (2003).
[23] W. Kittel and E. A. De Wolf, *Soft Multihadron Dynamics* (World Scientific, Hackensack, NJ, 2005), p. 652.
[24] Z. Chajecki (STAR Collaboration), AIP Conf. Proc. **828**, 566 (2006).
[25] N. M. Agababyan *et al.* (EHS/NA22 Collaboration), Z. Phys. C **71**, 405 (1996).
[26] M. Gazdzicki and S. Mrowczynski, Z. Phys. C **54**, 127 (1992).
[27] O. Utyuzh, G. Wilk, and Z. Wlodarczyk, Phys. Rev. D **75**, 074030 (2007).
[28] G. F. Bertsch, P. Danielewicz, and M. Herrmann, Phys. Rev. C **49**, 442 (1994).
[29] F. James, CERN-68-15, http://doc.cern.ch/cernrep/1968/1968-015/1968-015.html.
[30] H. Sorge, H. Stoecker, and W. Greiner, Nucl. Phys. **A498**, 567c (1989).
[31] R. Hagedorn, *Relativistic Kinematics* (Benjamin, New York, 1963), p. 166.
[32] E. Fermi, Prog. Theor. Phys. **5**, 570 (1950).
[33] S. Pratt, Phys. Rev. D **33**, 1314 (1986).
[34] G. Bertsch, M. Gong, and M. Tohyama, Phys. Rev. C **37**, 1896 (1988).
[35] P. Danielewicz and S. Pratt, Phys. Lett. **B618**, 60 (2005).
[36] P. Danielewicz and S. Pratt, Phys. Rev. C **75**, 034907 (2007).
[37] P. Danielewicz *et al.*, Phys. Rev. C **38**, 120 (1988).
[38] N. Borghini, P. M. Dinh, and J.-Y. Ollitrault, Phys. Rev. C **62**, 034902 (2000).
[39] N. Borghini, Eur. Phys. J. C **30**, 381 (2003).
[40] N. Borghini, Phys. Rev. C **75**, 021904(R) (2007).
[41] A. M. Poskanzer and S. A. Voloshin, Phys. Rev. C **58**, 1671 (1998).
[42] D. Brown and P. Danielewicz, Phys. Lett. **B398**, 252 (1997).
[43] Z. Chajecki (STAR Collaboration), Nucl. Phys. **A774**, 599 (2006).
[44] P. Avery *et al.*, Phys. Rev. D **32**, 2294 (1985).
[45] G. Abbiendi *et al.* (OPAL Collaboration), Eur. Phys. J. C **52**, 787 (2007).
[46] S. Chekanov *et al.* (ZEUS Collaboration), Phys. Lett. **B583**, 231 (2004).
[47] J. Adams *et al.* (STAR Collaboration), Phys. Rev. Lett. **91**, 262302 (2003).
[48] R. Lednicky, V. L. Lyuboshits, B. Erazmus, and D. Nouais, Phys. Lett. **B373**, 30 (1996).
[49] T. Sjostrand *et al.*, Comput. Phys. Commun. **135**, 238 (2001).
[50] M. A. Lisa *et al.* (E895 Collaboration), Phys. Lett. **B496**, 1 (2000).
[51] M. A. Lisa, U. W. Heinz, and U. A. Wiedemann, Phys. Lett. **B489**, 287 (2000).
[52] U. W. Heinz, A. Hummel, M. A. Lisa, and U. A. Wiedemann, Phys. Rev. C **66**, 044903 (2002).
[53] S. Chapman, P. Scotto, and U. W. Heinz, Phys. Rev. Lett. **74**, 4400 (1995).
[54] C. E. Shannon, Proc. Inst. Radio Eng. **37**, 10 (1949).
[55] A. J. Jerri, Proc. IEEE **65**, 1565 (1977).
[56] D. Brown (private communication).